ELSEVIER

MoS_2 and semiconductors in the flatland

Oleg V. Yazyev[1,*] and Andras Kis[2,*]

[1] Institute of Theoretical Physics, Ecole Polytechnique Fédérale de Lausanne (EPFL), CH-1015 Lausanne, Switzerland
[2] Electrical Engineering Institute, Ecole Polytechnique Fédérale de Lausanne (EPFL), CH-1015 Lausanne, Switzerland

The fascinating properties of graphene, the first two-dimensional (2D) material, and the accompanying strong activity in the research community have sparked a renewed interest in related layered crystalline materials with unique electronic and optical properties. Their superb mechanical properties, optical transparency, direct band gap and large degree of electrostatic control due to their atomic scale thickness make them interesting inorganic nanosystems for a wide variety of applications. In this review we will present a short history of research in the synthesis, band properties and potential applications of 2D semiconductors with a particular emphasis on MoS_2, the prototypical and best-studied material from this family.

Introduction

In addition to graphene and graphite, some of the best known layered materials are transition metal dichalcogenides (TMDs) with the common chemical formula MX_2 where M stands for a transition metal (M = Mo, W, Nb, Ta, Ti, Re) and X for S, Se or Te. Bulk TMD crystals are formed by vertical stacking of two-dimensional (2D) layers, separated by ~6.5 Å, Fig. 1a. TMD materials span a wide range of electronic properties from semiconducting to superconducting and metallic.

This class of materials has been studied extensively since 1960s in bulk, few-layer [1,2] or fullerene-like nanoparticle or nanotube [3–5] forms, mostly in the context of low-friction coatings and catalysis. It was the thinning down to single layers [6] and the availability of a wide range of techniques developed for graphene-related research that opened new perspectives for the study of 2D TMD layers. The interest in this new field was quickly sparked with the realization that single layers have electronic and optical properties different from bulk materials [7,8] and that they can be incorporated into high-quality electronic devices [9]. In this review, we will focus on the semiconducting, Mo and W-based, compounds from the TMD family with a particular emphasis on MoS_2, the most widely studied material of this type.

*Corresponding authors:. Yazyev, O.V. (oleg.yazyev@epfl.ch), Kis, A. (andras.kis@epfl.ch)

Material preparation

Chemical vapor transport

Bulk TMD crystals can be grown using the chemical vapor transport method, originally developed by Schäfer [13] where purified dichalcogenide material in the form of powder is mixed with the transport agent, usually bromine or iodine and sealed in a quartz ampoule. Pure component materials, for example W and Se for the growth of WSe_2 can also be used. The quartz ampoule is introduced into a zone electric furnace, with a temperature gradient maintained along the tube. A wide variety of TMD crystals including $MoSe_2$, $MoTe_2$, WS_2, WSe_2, $NbSe_2$, among others have been grown using this method [14–16].

Micromechanical cleavage

Mono and few-layer flakes of TMDs can be easily extracted from bulk crystals (Fig. 1b,c) in the same way that the first 2D material, graphene, was produced [6]. In addition to crystals produced using the chemical vapor transport method, MoS_2 crystals in the form of mineral molybdenite can be used for this purpose. This easy availability of MoS_2 is probably the main factor leading to most of the studies on 2D semiconductors being performed on this particular material.

The micromechanical cleavage method consists of applying an adhesive tape to the surface of the bulk crystal (Fig. 1b), peeling it off and applying the adhesive tape to a substrate cleaned of organic

1369-7021/ http://dx.doi.org/10.1016/j.mattod.2014.07.005

Please cite this article in press as: O.V. Yazyev, A. Kis, Mater. Today (2014), http://dx.doi.org/10.1016/j.mattod.2014.07.005

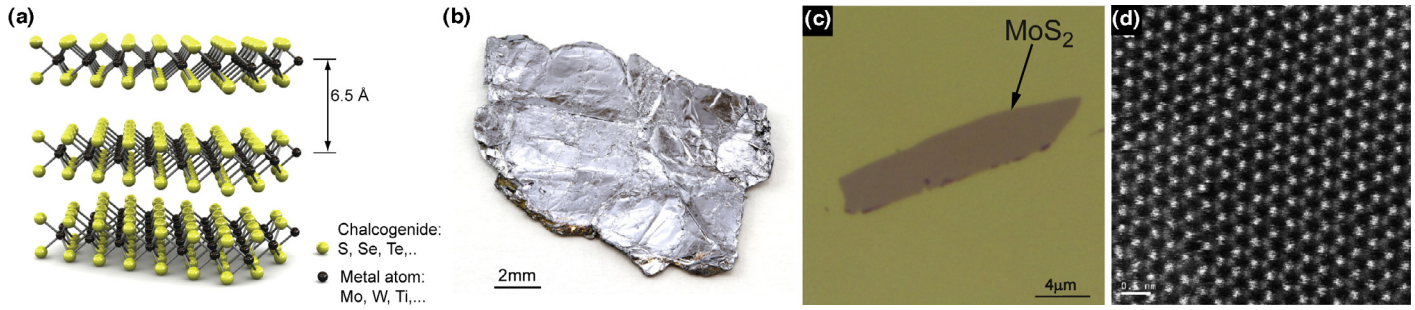

FIGURE 1

(a) Schematic representation of the structure of a TMD material with a formula MX_2 where metallic atoms are shown in black and chalcogens (X) in yellow [9]. (b) Photograph of a bulk crystal of MoS_2 that can be used as a starting point for the exfoliation of single layers [10]. (c) Optical image of a monolayer MoS_2 deposited on the surface of SiO_2 [11]. (d) Atomic resolution transmission electron microscopy (HAADF) image (raw data) of single-layer MoS_2 [12]. Reproduced from Refs. [9,11] with permission from Nature Publishing group. Adapted from Ref. [12] with permission from the American Chemical Society.

residue. 2D crystals suitable for integration into devices and further studies (Fig. 1c) can be easily identified by light interference [10,17]. This method produces flakes with sizes up to 10s of microns across and with high crystallinity (Fig. 1d) and quality that is sufficient for producing electronic devices and even simple circuits [18]. It requires the simplest of equipment in the form of a decent optical microscope. It is this simplicity that was one of the driving forces behind the rapid spreading of graphene and now MoS_2-related research. The main drawback is however the lack of scalability and the relatively tedious procedure of searching for interesting flakes under an optical microscope. For this reason, methods capable of producing large quantities of nanosheets are needed.

Liquid exfoliation

One of the most promising approaches for producing large quantities of single and few-layer nanosheets for applications in composites and inks is liquid-phase exfoliation. The relatively large separation between the sheets of layered materials allows intercalation with a variety of compounds including alkali metals. This approach [19] consists of soaking a powder or crystal of a layered material (in this case MoS_2) in a solution of butyl lithium in hexane, resulting in Li intercalation of MoS_2. The solution is then mixed with water, resulting in the release of gaseous hydrogen that pushes the layers apart. While this method can produce gram quantities of exfoliated monolayers, the resulting material is in the 1*T* metallic phase that needs to be heated to above 300°C to restore it to the semiconducting 2*H* polytype [19–21]. The use of lithium necessitates that the entire intercalation process is carried out in inert atmosphere. The alternative is to perform exfoliation by ultrasonication in organic solvents or surfactant solutions [22,23] with the surface tension of the solvent closely matched to the surface energy of the solid that is being exfoliated. The main advantage of liquid-phase exfoliation is that it can result in large quantities of monolayer dispersions that can be used for composite fabrication or monolayer material deposition by inkjet printing, spin coating or spraying. The resulting films are however composed of relatively small flakes. This limits their use in electronics or photonics applications where large and continuous films with small defect concentrations are required.

CVD growth

With the rapid growth of this research field, different methods for large-area growth became available already in early 2012, with pioneering results by Zhan et al. [26] and Liu et al. [27]. These methods are based on the use of solid materials such as Mo [26] or MoO_2 [28] which are first deposited in the form of thin films on substrates, and then subjected to reactions with sulphur at elevated temperatures. A different approach was used by Liu et al. who developed a synthesis method based on the thermal decomposition of ammonium-tetrathiomolybdate ($(NH_4)_2MoS_4$) [27] heated in the presence of sulphur. Although encouraging, these early methods were limited by the difficulty in achieving monolayer growth. The control over the thickness and monolayer growth over large areas was reported by Liu [29], Lou [24] and Hone groups

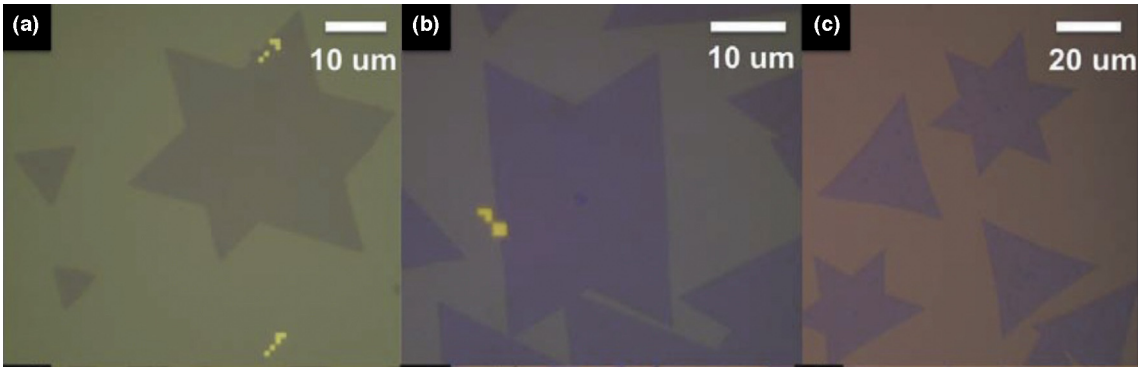

FIGURE 2

(a–c) Different shapes of monolayer MoS_2 grown by CVD based on solid-state precursors MoO_3 and sulphur [24,25]. Reproduced from Ref. [25] with permission from Nature Publishing group.

Please cite this article in press as: O.V. Yazyev, A. Kis, Mater. Today (2014), http://dx.doi.org/10.1016/j.mattod.2014.07.005

[25]. Their method is based on using solid MoO_3 and S powders, judiciously placed in a furnace and heater under inert gas flow at atmospheric pressure. The solid precursors evaporate and react in the vapor phase. The growth results in single-grain domains one layer thick (Fig. 2) with typical size on the order of 100 μm and electronic and optical properties similar to exfoliated samples. Growth of WS_2 using a similar method has also been recently reported by the Terrones group [30]. More effort is still needed to increase the area over which films uniformly grow and to introduce various *p* and *n*-type dopants during growth.

Properties

Electronic structure

Electronic structure calculations have been playing an important role in understanding the physical properties of monolayer MoS_2 and isostructural TMDs. In particular, the workhorse first-principles methodology based on density functional theory (DFT) [31–33] has been extensively used. This computational approach commonly utilizes the following two forms of the so-called exchange correlations functional: the local density approximation (LDA) [34] and the generalized gradient approximation (GGA) [35]. More recently, several groups reported first-principles results based on highly accurate but computationally demanding many-body perturbation theory techniques. These calculations employed the *GW* approximation [36,37] for predicting the quasiparticle band structures and the Bethe–Salpeter equation (BSE) approach [38,39] for optical spectra.

Electronic structure calculations provide an important insight into the evolution of band structure upon changing the number of layers from bulk materials down to monolayers. Figure 3a,b shows

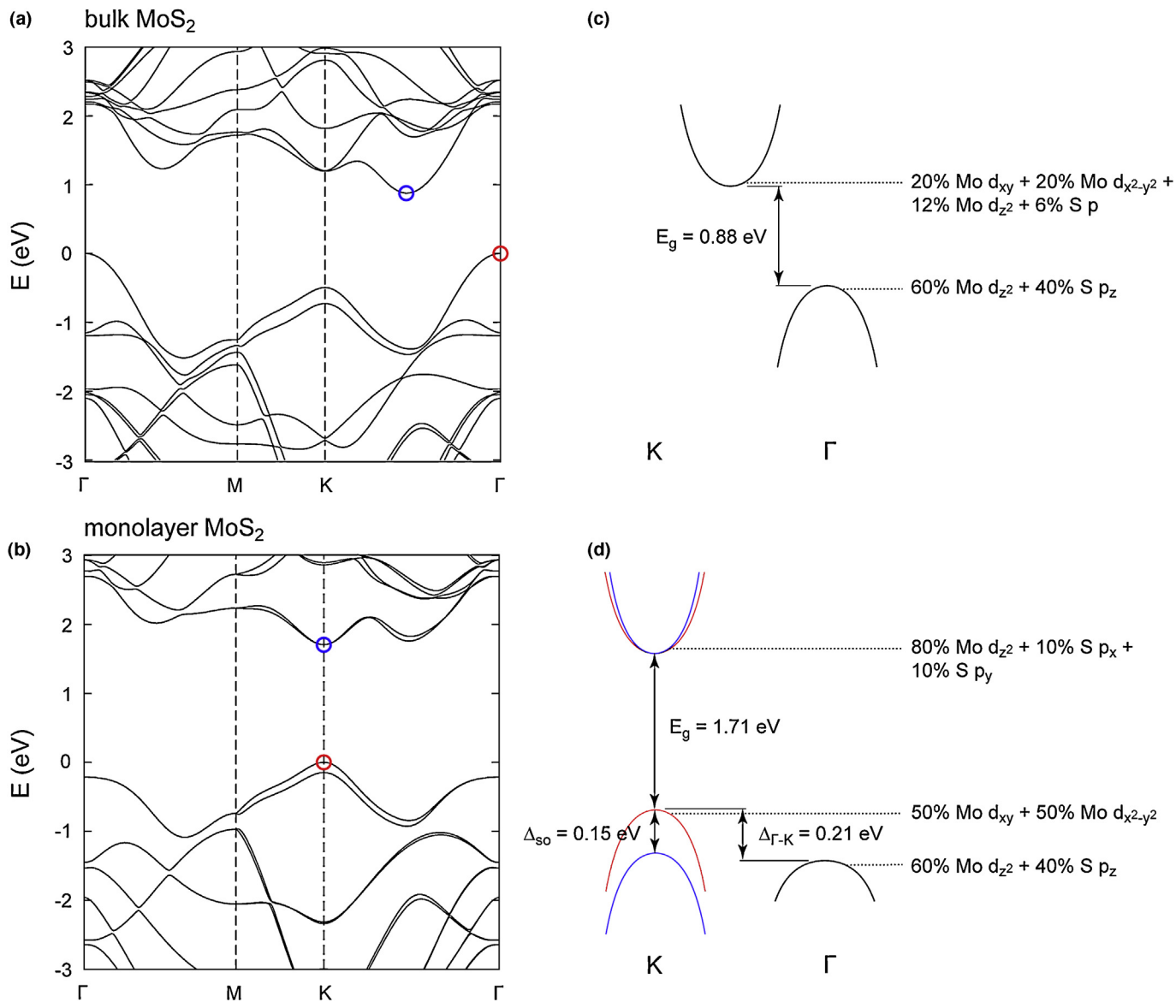

FIGURE 3

Electronic band structures of (a) bulk MoS_2 and (b) monolayer MoS_2 calculated from first principles using density functional theory (DFT) within the generalized gradient approximation (GGA). Valence band maxima (VBM) and conduction band minima (CBM) are indicated by red and blue circles, respectively. Energies are given relative to the VBM. Schematic drawings of low-energy bands in (c) bulk MoS_2 and (d) monolayer MoS_2 showing the band gaps E_g as well as the valence band spin–orbit splitting Δ_{so} and the Γ valley band offset $\Delta_{\Gamma\text{-}K}$ for the case of monolayer MoS_2. The band structure parameters have been obtained at the DFT–GGA level of theory. The orbital composition of electronic states at band extrema is indicated.

Please cite this article in press as: O.V. Yazyev, A. Kis, Mater. Today (2014), http://dx.doi.org/10.1016/j.mattod.2014.07.005

the band structures of bulk and monolayer MoS_2, respectively, calculated using conventional DFT–GGA approach. Bulk MoS_2 is an indirect gap semiconductor with valence band maximum (VBM) located at the Γ point and conduction band minimum (CBM) located at a low-symmetry point of the Brillouin zone (Fig. 3a). Schematic illustration of the band structure of bulk MoS_2 shown in Fig. 3c indicates the theoretical value of band gap of 0.88 eV obtained using DFT–GGA. Experimental value of the band gap of bulk MoS_2 is 1.2 eV [40]. We note that the Kohn–Sham DFT, employing either LDA or common GGA exchange correlation functionals, has a tendency to systematically underestimate band gaps, while more advanced methods like the *GW* approximation are largely free of this deficiency [41]. The shapes of valence and conduction bands undergo significant changes upon decoupling MoS_2 layers. In particular, the positions of both VBM and CBM of monolayer MoS_2 shift to the *K* point making it a direct gap semiconductor (Fig. 3b,d) [42,43]. The band gap obtained from DFT–GGA calculations is 1.71 eV while its optically measured value is 1.9 eV [8,7]. However, it is worth noting that the Γ valley of the valence band is separated from the VBM by a relatively small offset $\Delta_{\Gamma-K}$ (0.21 eV according to DFT–GGA calculations).

These striking changes of the band structure upon reducing the number of layers are directly related to the orbital composition of involved electronic states. At the *K* point, the valence and conduction band states are mostly composed of localized *d* orbitals of the Mo atoms (Fig. 3c,d). These electronic states are relatively insensitive to interlayer coupling. However, there is a large contribution of *p* orbitals of the S atoms to the electronic states at the Γ point. This makes both the valence and conduction bands at the Γ point strongly affected by the quantum confinement effects. The difference of the band gap character of bulk and monolayer MoS_2 has been confirmed by means of optical measurements [7,8]. In particular, monolayer MoS_2 shows four orders of magnitude larger luminescence quantum efficiency compared to bulk material. More recently, angle-resolved photoemission spectroscopy (ARPES) measurements provided direct access to the dispersion of valence band confirming the predicted shift of the VBM from Γ to *K* upon reducing the thickness of MoS_2 films to a single layer [44].

Other MX_2 materials (M = Mo, W; X = S, Se, Te) exhibit qualitatively very similar electronic properties. According to DFT calculations all monolayer MX_2 semiconductors have direct band gaps in the range 1–2 eV. Table 1 provides a representative, albeit not complete, overview of band structure parameters of semiconducting MX_2 monolayers obtained from first principles using DFT (GGA) and the *GW* approximation approaches. These predictions show that replacing Mo by W leads to somewhat larger band gaps while going down the periodic table along the S–Se–Te series reduces the band gap. Increasing the weight of atomic components results in the increase of Γ-to-*K* energy difference $\Delta_{\Gamma-K}$.

Enhancing the functionality of 2D TMD materials for electronic and optoelectronic applications requires a strategy for band gap tuning. This would allow closer matching of optoelectronic devices such as solar cells, photodetectors or light-emitting diodes (LEDs) to a particular application. In analogy with the InGaAs system, the band gap in MX_2 materials can also be tuned by mixing two compounds with different band gaps, for example $MoSe_2$ (E_g = 1.5 eV) and $MoTe_2$ (E_g = 1.1 eV) in $MoSe_{2x}Te_{2(1-x)}$. Theoretical models [45] predict that these materials form random substitutional alloys that are thermodynamically stable. The direct nature of the band gap is preserved and its magnitude can be continuously tuned, in the case of Mo–Se–Te from 1.1 eV to 1.5 eV, by changing the mixing ratio *x*. Such band gap tuning by alloying was demonstrated in the monolayer $Mo_{1-x}W_xS_2$ system [46] and in $MoS_{2(1-x)}Se_{2x}$ [47,48]. The unique properties of 2D dichalcogenides, namely their atomic scale thickness and high mechanical strength [49] allow two additional strategies for tuning the band

TABLE 1

Band structure parameters of monolayer MX_2 materials calculated from first principles.

Material	E_g (eV)	$\Delta_{\Gamma-K}$ (meV)	Δ_{so} (meV)	Method	Ref.
MoS_2	1.67			DFT–GGA	[69]
		50	148	DFT–GGA	[59]
	2.82		164	GW	[70]
	2.75	160		GW	[71]
$MoSe_2$	1.44			DFT–GGA	[69]
		360	183	DFT–GGA	[59]
	2.41		212	GW	[70]
	2.33	340		GW	[71]
$MoTe_2$	1.07			DFT–GGA	[69]
	1.77		266	GW	[70]
	1.82	830		GW	[71]
WS_2	1.81			DFT–GGA	[69]
		220	426	DFT–GGA	[59]
	2.88		456	GW	[70]
	2.88	60		GW	[71]
WSe_2	1.55			DFT–GGA	[69]
		530	456	DFT–GGA	[59]
	2.34[a]		501	GW	[70]
	2.38	340		GW	[71]
WTe_2	1.06			DFT–GGA	[69]
	1.77	790		GW	[71]

[a] Monolayer WSe_2 is an indirect gap semiconductor according to the GW calculation of Ref. [70]. The direct gap at point *K* is 2.42 eV.

Please cite this article in press as: O.V. Yazyev, A. Kis, Mater. Today (2014), http://dx.doi.org/10.1016/j.mattod.2014.07.005

gap in TMD materials. First is based on applying a perpendicular electric field to bilayer MX_2 [50]. This is analogous to an opening of band gap in bilayer graphene [51]. However, in contrast to graphene where applying the electric field results in band gap opening that saturates at around 0.25 eV, here the band gap is predicted to completely close for similar magnitudes of external electric field, on the order of 2–3 V/nm. Mechanical strain could also be used to tune the band gap of monolayer TMDs. Depending on the nature of strain (uniaxial, uniform, biaxial) and modeling approach used, MoS_2 and other semiconducting MX_2 monolayers are expected to show either a decrease of band gap from ~2 eV to 1.1 eV [52] or a complete closing of the band gap and transition into a metallic state [53,54] (Fig. 4a) possibly accompanied by a change from a direct to an indirect semiconductor [55].

First experimental observations that confirm the possibility of band gap tuning by strain have already been published, with maximum strains on the order of 1–2% and an accompanying band gap decrease of ~45 meV/% strain [56,57] (Fig. 4b,c). Local strain induced by depositing MoS_2 on a prestretched substrate (Fig. 4d) was also shown to result in a similar band gap decrease and an influence over the position along the locally strained flake in which photoluminescence occurs [58]. The observed breaking strength of 11% [49] could make complete band gap closure possible [53].

Manifestations of spin–orbit coupling in the electronic properties of monolayer TMDs are another important subject of theoretical and experimental studies. Bulk MoS_2 in its 2*H* phase as well as even-layer thin films of this material are centrosymmetric. By contrast, monolayer MoS_2 has a noncentrosymmetric crystal structure. The lack of inversion symmetry results in lifting the spin degeneracy of electronic bands due to spin–orbit interaction. This effect is particularly pronounced in the valence band of monolayer MoS_2 giving rise to spin splitting $\Delta_{so} = 0.15$ eV according to DFT–GGA calculations (Fig. 3b,d) [59]. The spin splitting is even larger for other monolayer MX_2 materials as being a relativistic effect the strength of spin–orbit coupling increases rapidly with increasing atomic number of constituent elements (Table 1). For instance, first-principles calculations predict $\Delta_{so} = 0.46$ eV for monolayer WSe_2 [59]. Although weaker, spin–orbit effects are also present in the conduction band states. The spin–split conduction bands are characterized by somewhat different effective masses (Fig. 3b,d) and energy splittings of the order of meVs.

Spin–orbit effects make monolayer TMDs interesting from the point of view of applications beyond traditional electronics. Strong spin splitting of the valence bands would allow using these materials in spintronics – extension of electronics operating the spin degree of freedom of electrons for storing and manipulating information [60,61]. Even more interesting is the fact that the valence and conduction bands of MX_2 monolayers are arranged into two inequivalent valleys at points *K* and *K′*. This peculiarity makes these materials attractive for valleytronics manipulating the valley degree of freedom of charge carriers [62,63]. The combination of two-valley physics with strong spin–orbit effects results in spin–valley coupling, resulting in for example a property which can be further exploited in future beyond-electronics devices [64].

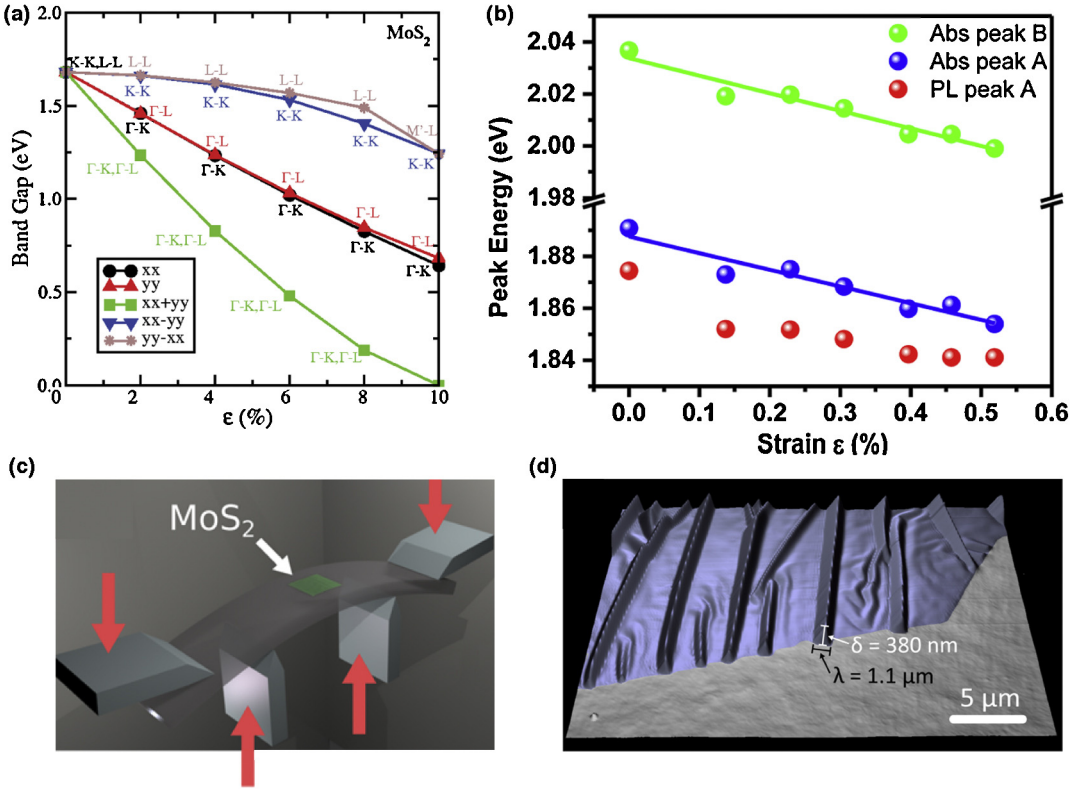

FIGURE 4

Strain-induced band gap tuning in MoS_2. (a) Calculated band gap of monolayer MoS_2 with respect to strain with deformation in various directions [53]. (b) Experimentally observed variation of the A and B exciton peak energies in monolayer MoS_2 for different values of strain up to 0.5% [56]. (c) Schematic drawing of the beam bending apparatus used to induce strain in MoS_2 deposited on a flexible substrate [57]. (d) Atomic force microscope image of winkled MoS_2 produced by exfoliation on top of a prestretched elastomeric substrate [58]. Adapted from Refs. [56,57] with permission from the American Chemical Society.

First steps in this direction have already been demonstrated. Valley polarization was induced optically using circularly polarized light and detected using circularly polarized photoluminescence [65–67] and the valley Hall effect [68].

Electrical properties

The presence of a band gap in 2D semiconductors indicates that they could have advantages for use in electronic and logic circuits that are based on field-effect transistors. One of the key requirements for building a useable field-effect transistor is the ability to turn it off by applying a voltage to the control, gate electrode. 2D semiconductors are well-suited for this purpose, as the presence of a band gap allows the material to be depleted of charge carriers. The atomic scale thickness is also a huge advantage compared to '3D' materials such as silicon because it can reduce short-channel effects. They degrade the performance of nanometer-sized transistors and result from the penetration of the electric field due to contacts into the semiconducting channel. The penetration length can be described by a parameter called natural length λ:

$$\lambda = \sqrt{\frac{\varepsilon_{ch}}{\varepsilon_{ox}} d_{ch} d_{ox}} \quad (1)$$

where ε_{ch} and ε_{ox} are dielectric constants of the channel and the oxide and d_{ch} and d_{ox} are thicknesses of the semiconducting channel and the oxide. To make a device that is not dominated by short-channel effects, the channel length needs to be at least 3–4× longer than λ. From this, it is clear that thin materials present an advantage and that 2D semiconductors like the monolayer TMDs, at the ultimate limit of thickness would allow a very high degree of electrostatic control [72,73]. The 2D nature of the semiconducting channel is also interesting for the realization of sensors biosensors where pH sensing and specific protein sensing has been demonstrated using MoS_2 [74].

While some of the semiconducting properties of TMD materials have been known since the 60s and the first paper reporting exfoliation of thin MoS_2 was published in 1963 by Frindt et al. [1], this class of materials was not being considered for electronics-related applications in spite of mobility measurements showing in-plane mobility in bulk MoS_2 and WSe_2 exceeding 100 cm^2/V s [75] at room temperature. First transistors based on bulk WSe_2 were reported in 2004 but they showed a low on/off ratio (~10) because of conduction through the bulk which was not controlled by the gate electrode. The first device based on single-layer MoS_2 [6] was demonstrated soon after the seminal work on graphene by Novoselov and Geim in 2005. It had a mobility of ~3 cm^2/V s and a relatively low on/off ratio [6]. First successful demonstration of a switchable transistor based on monolayer MoS_2 by Radisavljevic et al. in 2011 (Fig. 5a) [9] brought the attention to MoS_2 and TMDs in the context of electronics. Their device showed a room-temperature on/off ratio of ~10^8, a negligible off-state current and *n*-type transport (Fig. 5b). The device was realized in a top-gated geometry which allows the local control over conductivity in a similar way as in commercial FETs, making the integration of multiple devices on the same substrate feasible. Later monolayer MoS_2 FETs showed saturation and maximal current densities of ~170 μA/μm [76], exceeding the current-carrying capacity of copper by a factor of 50. Current saturation and mobility >100 cm^2/V s was also demonstrated in slightly thicker multilayer MoS_2 structures [77].

Similar devices were later realized based on monolayer WSe_2 with *p*-type FETs exhibiting a room temperature hole mobility of 250 cm^2/V s and an on/off ratio of 10^6 [78] and *n*-type transistors with an electron mobility of 142 cm^2/V s [79]. Ambipolar transport has also been demonstrated in 10 nm thick MoS_2 using liquid ionic gating [80] as well as in WS_2 where the high capacitance of the liquid ion-based gate allowed the direct electrical measurement of the band gap of this material for monolayer, bilayer [81] and thin flims of 20–60 nm range of thickness [82]. Liquid ionic gating was also used to achieve high doping levels in MoS_2 resulting in observation of superconductivity with a gate tunable transition temperature showing a maximum at 11 K [83].

One of the key breakthroughs that allowed the fabrication of monolayer MoS_2 transistors was the realization that embedding them in a high-κ dielectric film in the form of HfO_2 can increase the mobility by effectively decreasing charged impurity scattering as well as photon scattering [84]. Another complementary approach to achieving high mobility is to perform vacuum annealing which presumably results in the removal of adsorbates and fabrication-related residue that act as charged impurities [85,86]. This lead to reports of ~250 cm^2/V s Hall effect and ~1000 cm^2/V s field-effect effective mobilities in monolayer MoS_2 at low

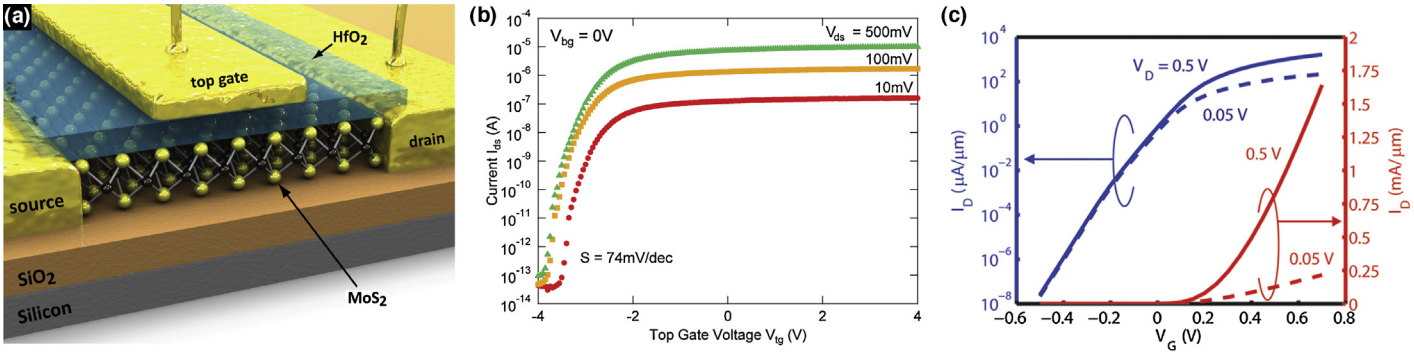

FIGURE 5

Monolayer MoS_2 transistors. (a) Schematic representation of the first top-gated MoS_2 field-effect transistor. Reproduced from Ref. [88] with permission from Nature Publishing group. (b) The device current as a function of gate voltage. The device can be completely turned off for gate voltages <−2 V. The I_{On}/I_{Off} ratio is >1 × 10^8 [9]. Reproduced from Ref. [9] with permission from Nature Publishing group. (c) Simulated device characteristics for a monolayer MoS_2 FET device with 2.8 nm thick HfO_2 top gate oxide, 15 nm gate length and power supply voltage 0.5 V [72]. Adapted from Ref. [72] with permission from the American Chemical Society.

Please cite this article in press as: O.V. Yazyev, A. Kis, Mater. Today (2014), http://dx.doi.org/10.1016/j.mattod.2014.07.005

temperatures and charge densities $>10^{13}$ cm^{-2} [85] as well as reduced $1/f$ noise [87].

Theoretical models predict that at room temperature the mobility is expected to be limited by phonon scattering with the upper limit ranging from 130 to 410 cm^2/V s [89–93]. The performance of MoS_2 and 2D TMD transistors is currently also limited by the presence of band tail trapping states that were recently quantified by the Avouris group using capacitance and ac conductance measurements [94]. Charges trapped in these states can also lead to an underestimation of the band mobility. An additional source of scattering could be the ripples [95], local height fluctuations that could also reduce the conductivity of MoS_2 [96].

Simulations also show that monolayer MoS_2 and by extension other monolayer TMDs would have high resistance to short-channel effects due to its small thickness [72,73] and would maintain their high on/off ratio for small channel lengths (Fig. 5c). Measurements on multilayer devices with channel lengths in the sub-100 nm range have confirmed the absence of short-channel effects at this scale [97,94]. Further scaling could be achieved by reducing the contact resistance in these devices, for example by using scandium contacts [98].

Transistors were also incorporated into simple electronic circuits capable of performing basic operations. The first and simplest such circuit was composed of two transistors realized on the same piece of MoS_2 and connected in series in the way depicted in Fig. 6a. Here, the 'lower' transistor acts as a switch and the 'upper' one as a resistor. One of the main features of this device is its switching slope which defines its gain, higher than 4 in this case (Fig. 6c). The gain should be higher than 1 so that multiple logic gates could be incorporated into more complicated circuits. The same device can also be operated as an analog amplifier [99] allowing the amplification of small analog signals. Logic circuits based on bilayer MoS_2 such as ring oscillators and random access memory were demonstrated by Wang et al. [100]. Another type of memory, in the form of flash memory, currently used in practically every consumer electronic device, from USB memory sticks, cell phones, digital cameras was demonstrated by Bertolazzi et al. [101]. The main building block of such memory circuits is the floating gate transistor, a device with a structure similar to a standard FET except that it incorporates an additional, electrically disconnected gate electrode placed between the conductive channel and the control gate electrode. Depending on the values of voltages applied to the different electrode in the device, charges can be stored and transferred between the floating gate and the channel. The presence of charges stored on the floating gate can then screen the charge from the control gate and modify the response of the transistor, allowing the device to function as a memory cell.

One of the main problems limiting the scaling of current flash memory devices is the reduction in the amount of charge that can be stored on the floating gate as its size is reduced. Crosstalk between neighboring memory cells also increased as the distance between the cells is decreased. Both of these problems could be addressed by using 2D materials: the large degree of electrostatic control over conductivity in 2D channels means that they would be more sensitive to a small amount of charge stored on the floating gate than their 3D counterparts. The reduced thickness will also decrease capacitive coupling between neighboring cells, enabling higher packing densities.

Such a device was built by Bertolazzi et al. (Fig. 7a) using 2D materials for several important components. The transistor channel was composed of monolayer MoS_2 contacted with graphene electrodes (Fig. 7b) that work as ohmic contacts with efficient charge injection from graphene into MoS_2. This shows that graphene could be used as a high-quality contact to MoS_2 and related 2D semiconductors which could be interesting for the fabrication of transparent and flexible electronic circuits. The floating gate, responsible for storing charge was also made out of four-layer graphene, chosen because it has a larger charge storage capacity compared to monolayer graphene. Because of its 2D nature, monolayer MoS_2 is very sensitive to the presence of charges in the charge trapping layer, resulting in a factor of 10^4 difference in currents between states in which the memory is stored and erased. The authors also estimate that the device could retain 30% of the stored charge after 10 years, an encouraging number given that this is the first device of its kind incorporating 2D materials.

Optoelectronic devices

Graphene is not just a thin form of graphite but a new material with properties that set it apart from its thicker counterparts. In the

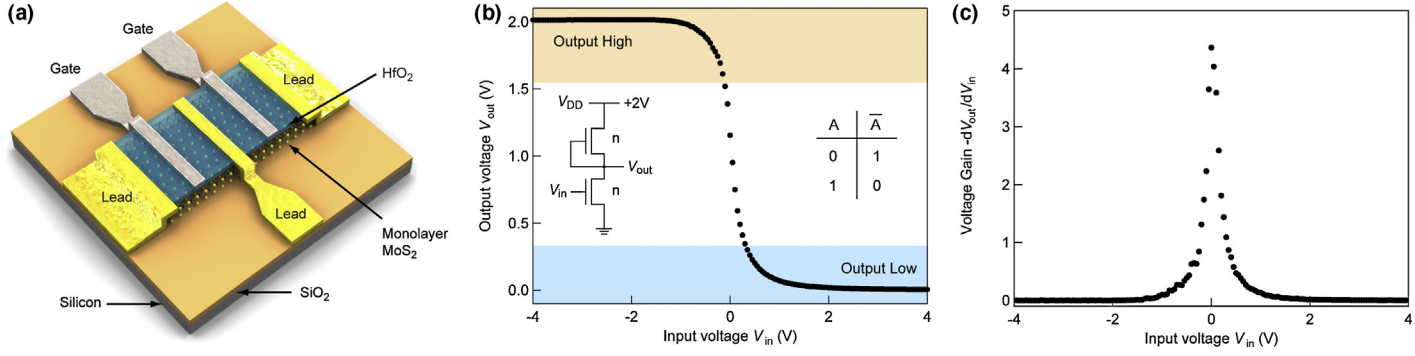

FIGURE 6

First monolayer MoS_2-based circuits. (a) Schematic representation of the integrated circuit based on monolayer MoS_2 composed of two transistors defined by a neighboring pair of leads and controlled using local gates deposited on the surface of the HfO_2 gate dielectric. (b) Output voltage as a function of the input voltage in the circuit. Schematic drawing of the electronic circuit and the truth table for the NOT logic operation (inset). (c) The dependence of the inverter gain (negative value of dV_{out}/dV_{in}) on the input voltage. Adapted from Ref. [18] with permission from the American Chemical Society.

Please cite this article in press as: O.V. Yazyev, A. Kis, Mater. Today (2014), http://dx.doi.org/10.1016/j.mattod.2014.07.005

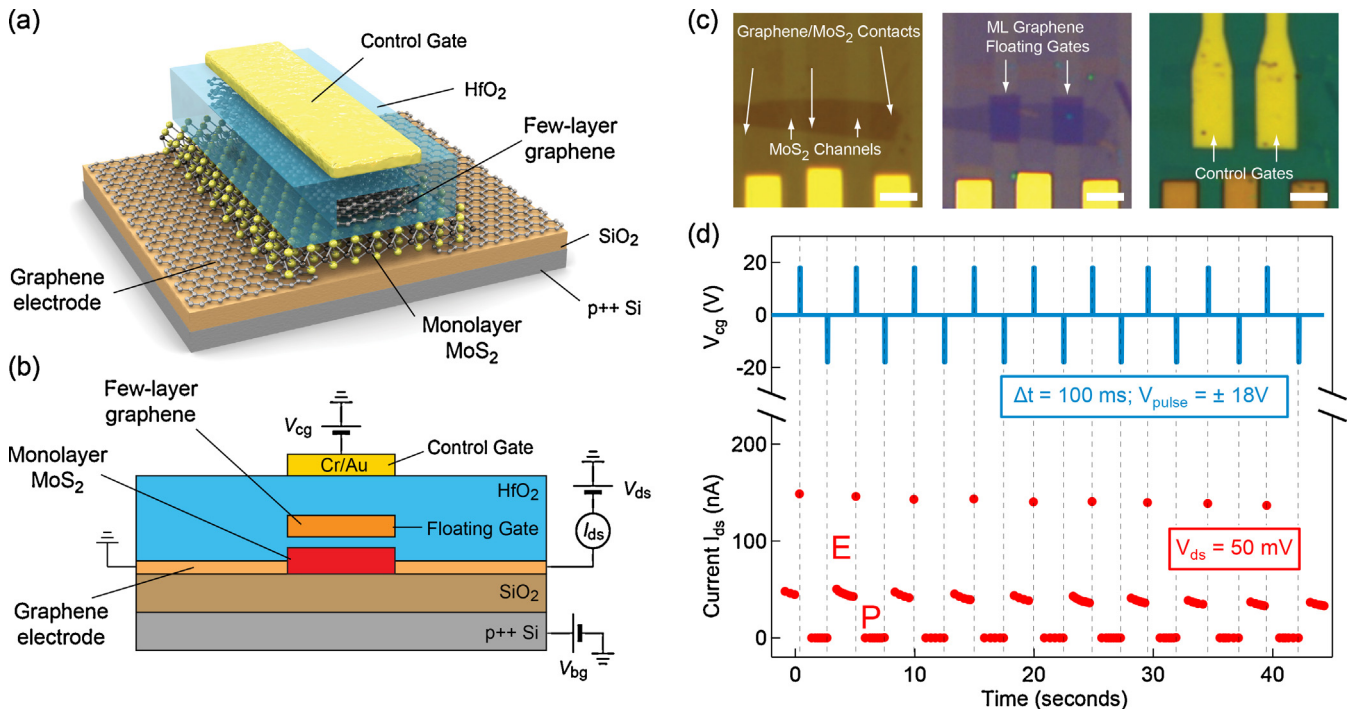

FIGURE 7

MoS_2/graphene heterostructure memory. (a) Representation of the device based on a MoS_2 transistor with graphene contacts and few-layer graphene floating gate. (b) Schematics of the connections used to characterize the device. (c) Optical images of two heterostructure devices during various stages of fabrication. Left: monolayer MoS_2 is placed over graphene stripes acting as contacts; middle: few-layer graphene is placed over MoS_2 covered with a thin layer of HfO_2; right: the finished device after top gate deposition. (d) Switching characteristic of the memory device. Adapted from Ref. [101] with permission from the American Chemical Society.

same way, single layers of TMD materials are fundamentally different from thicker crystals of bulk materials with the same chemical composition. First indication of this came with the realization that the band gap of MoS_2 changes from the bulk value of 1.2 eV [40] to 1.8 eV [8] as the thickness is decreased down to a monolayer (see section 'Electronic structure'). In the case of MoS_2, this is manifested by strong photoluminescence from monolayers [7,8] which indicates that this class of materials could be interesting for applications in optoelectronic devices such as LEDs, lasers, optical switches, photodetectors, modulators, displays, among others. Simple optoelectronic devices based on MoS_2 have already been demonstrated (Fig. 8). The first phototransistor based on monolayer MoS_2 (Fig. 8a) was shown to have a photoresponsivity of 7.5 mA/W [102], similar to graphene-based devices. By using MoS_2 layers of different thicknesses, photodetection can be turned to different wavelengths. Lee et al. have demonstrated that single- and double-layer MoS_2, with respective band gap energies of 1.8 and 1.65 eV can be used for detecting green light, and triple-layer MoS_2 with an indirect band gap of 1.35 eV is well-suited for red light detection [103]. Monolayer MoS_2 phototransistors with the high photoresponsivity of 880 A/W were reported by Lopez-Sanchez et al. [104] (Fig. 8b). The 2D nature of MoS_2 and the associated high degree of electrostatic control in this device allows very low dark currents, corresponding to the off-state current in the device, resulting in low dark current noise, one of the factors determining the detection limit of photodetectors. This gives rise to a very low noise equivalent power (NEP) of 1.5×10^{-15} W $Hz^{-1/2}$ in this device, which is more than an order of magnitude improvement over state-of-the-art commercial Si avalanche photodiodes [105]. While the photoresponse in these devices was determined by direct photoexcitation in the semiconducting channel, MoS_2–metal junctions can also show a strong photothermoelectric effect that can be tuned using an external electric field [106] and which could be used for thermopower generation. Optoelectronic devices based on MoS_2 can also emit light in electroluminescent devices with light emission occurring due to hot carrier processes in a region near locally gated contacts, as demonstrated by Sundaram et al. [107] (Figs 8c and 7d). Another way of generating light in 2D materials involves the realization of lateral *p–n* junctions, for example using monolayer WSe_2 where light emission and photodetection were also recently demonstrated [108–110].

First optoelectronic devices that exploit the spin–valley coupling were also demonstrated. They consist of *p–n* junctions realized within ultrathin WSe_2 and MoS_2 gated by liquid electrolytes and operating as LEDs [111]. The application of in-plane electric field allows valley symmetry breaking for electrons and holes due to trigonal warping [112,113], resulting in valley polarization reaching 45% and the emission of circularly polarized light.

Hybrid devices combining the advantages of graphene and TMDs in vertical heterostructures are another promising approach to realizing vertical devices with TMD layers incorporated in a sandwich between two graphene electrodes [114–116]. Such devices were recently shown to have a photoresponsivity of ~0.1 A/W and external quantum efficiency for light conversion of 30% [116]. Combining different TMD monolayers in vertical heterostructures, for example MoS_2 and WS_2 could also

Please cite this article in press as: O.V. Yazyev, A. Kis, Mater. Today (2014), http://dx.doi.org/10.1016/j.mattod.2014.07.005

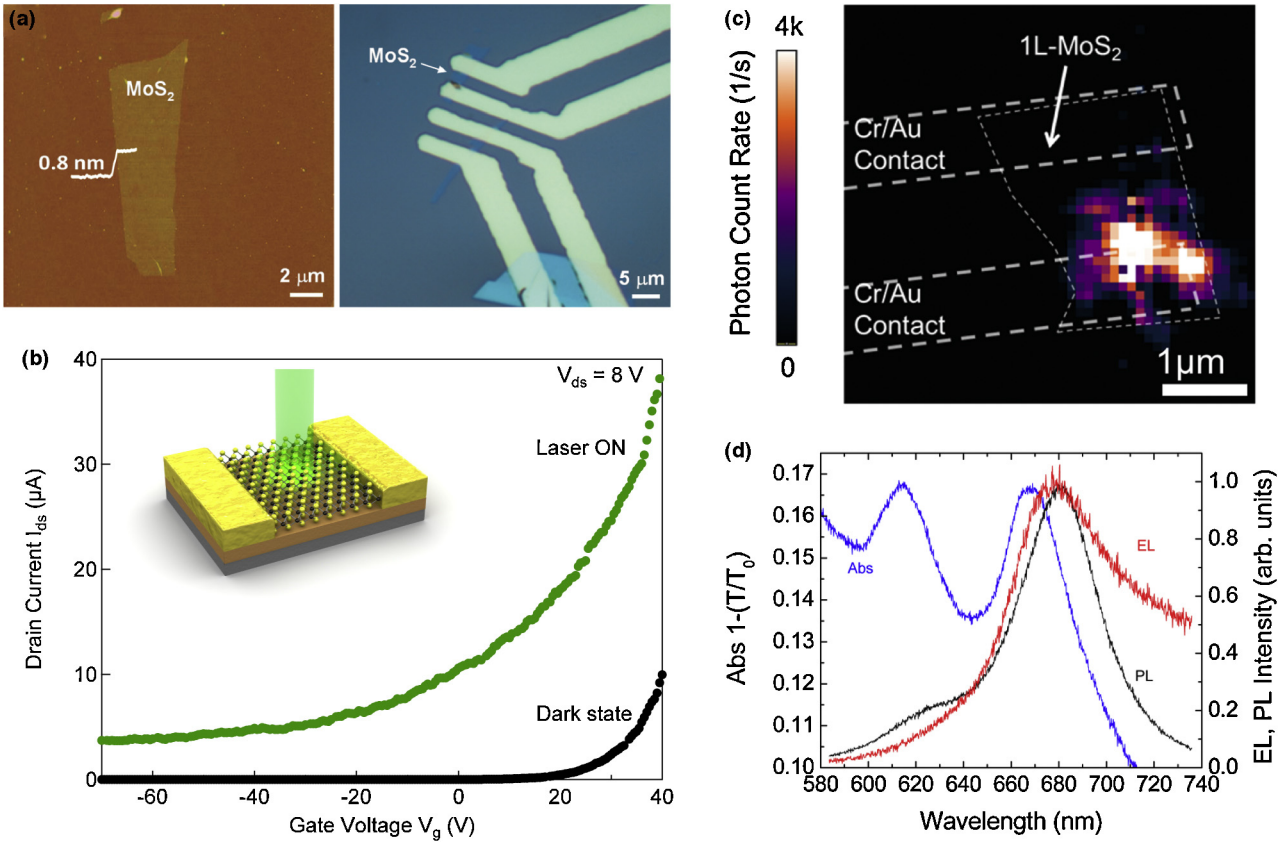

FIGURE 8

MoS_2-based optoelectronic devices. (a) Optical micrograph of a monolayer MoS_2 flake used to prepare the first MoS_2 phototransistor [102]. (b) Gating response of the ultrasensitive MoS_2 photodetector with a responsivity of 880 A/W. Reproduced from Ref. [104] with permission from Nature Publishing group. (c) False color image showing electroluminescence intensity in the vicinity of a contact edge. The positions of Cr/Au contacts are highlighted by thick dashed lines (white) and the MoS_2 layer is indicated by thin dashed lines (gray) [107]. (d) Absorbance, photoluminescence and electroluminescence spectrum recorded on the first MoS_2 light-emitting device [107]. Adapted from Refs. [102,107] with permission from the American Chemical Society.

lead to the realization of excitonic solar cells [117] where WS_2 would behave as a donor and MoS_2 as an acceptor in a type-II heterostructure.

Mechanical properties

First mechanical measurements performed on suspended membranes of monolayer MoS_2 deformed by an AFM tip show that it has a Young's modulus of ~270 GPa (in plane stiffness of ~180 N/m) [49], comparable to that of stainless steel. The ultimate tensile strength is ~23 GPa which is ~30× higher than in steel, due to the strong covalent bonds between transition metal and chalcogen atoms, with MoS_2 monolayers breaking at an effective strain in the 6–11% range. Density functional calculations of the mechanical response of MoS_2 and other 2D monolayers show that they all share such favorable mechanical properties, with the maximum breaking strain that could reach ~30% [118]. These mechanical properties make MoS_2 suitable for integration with flexible substrates such as polyimide that has a similar breaking strain. First flexible transistors based on multilayer MoS_2 have already been demonstrated using ion gel dielectrics [53], HfO_2 or Al_2O_3 [119,120] and BN as dielectrics [121]. The reported devices shown high current on/off ratios up to the smallest reported curvature radius of 0.75 mm [122]. Flexible transistors based on WS_2/graphene heterostructures showing 10^6 on/off ratios under at least 5% bending strain have also been recently reported [115]. Single-layer MoS_2 was also incorporated into nanomechanical resonators [123] with resonant frequencies in the 10–30 MHz range and quality factors ~55 measured at room temperature and in vacuum, together with nonlinear response for high driving powers.

Summary and prospects

We have reviewed here recent efforts in exploring the basic properties ultrathin TMD materials in the context of electronic materials, with the main emphasis on monolayer MoS_2 as the prototypical material from this family. Recent three years have seen a dramatic expansion of research effort in this class of materials with promising properties both for practical applications and fundamental studies in electronic and optoelectronic circuits as well as new physics related to spin–valley coupling. Combining different 2D materials into van der Waals heterostructures is another very promising research avenue [124]. The unique advantages of optical transparency, direct band gap and interesting electronic properties could make 2D semiconductors the materials of choice for the next generation of inexpensive and low-power electronic circuits, flexible and transparent solar cells and displays or wearable computing devices. To continue at this pace of progress, several issues need to be addressed in the near future. For

Please cite this article in press as: O.V. Yazyev, A. Kis, Mater. Today (2014), http://dx.doi.org/10.1016/j.mattod.2014.07.005

example, there is presently no control over intrinsic doping levels in MoS_2 and related materials, so methods for introducing dopant atoms in TMD monolayers as well as achieving ambipolar and *p*-type behavior in monolayer MoS_2 would be highly desirable. Understanding how to make good electrical contacts to MoS_2 is also lagging and it is not clear yet which material and contacting scheme would result in the smallest possible contact resistance. On the basis of theoretical predictions [90] there is also a lot of opportunity for improving the charge carrier mobility.

Contributions from physics, chemistry, materials science, electrical engineering and other disciplines have the potential to provide new advances in fundamental science and applications as well as on future technology.

Acknowledgements

We are grateful to G. Autès for his help with the band structure plots. O.V.Y. was supported by the Swiss National Science Foundation (grant no. PP00P2_133552) and the ERC Starting Grant no. 306504 (project 'TopoMat'). A.K. would like to acknowledge financial support by ERC grant no. 240076 (Flatronics: Electronic devices based on nanolayers), Swiss Nanoscience Institute (NCCR Nanoscience) grant no. 115482, and Swiss National Science Foundation (grant nos. 122044, 132102 and 138237).

References

[1] R.F. Frindt, A.D. Yoffe, Proc. R. Soc. A 273 (1352) (1963) 69.
[2] R.F. Frindt, J. Appl. Phys. 37 (4) (1966) 1928.
[3] R. Tenne, et al. Nature 360 (6403) (1992) 444.
[4] Y. Feldman, et al. Science 267 (5195) (1995) 222.
[5] R. Tenne, A.K. Zettl, Top. Appl. Phys. 80 (2001) 81.
[6] K.S. Novoselov, et al. PNAS 102 (30) (2005) 10451.
[7] A. Splendiani, et al. Nano Lett. 10 (4) (2010) 1271.
[8] K.F. Mak, et al. Phys. Rev. Lett. 105 (13) (2010) 136805.
[9] B. Radisavljevic, et al. Nat. Nanotechnol. 6 (3) (2011) 147.
[10] M.M. Benameur, et al. Nanotechnology 22 (12) (2011) 125706.
[11] Q.H. Wang, et al. Nat. Nanotechnol. 7 (11) (2012) 699.
[12] R. Zan, et al. ACS Nano 71 (11) (2013) 10167.
[13] H. Schäfer, Chemical Transport Reactions, Academic Press, New York, 1964.
[14] L.H. Brixner, J. Inorg. Nucl. Chem. 24 (3) (1962) 257.
[15] R. Nitsche, J. Phys. Chem. Solids 17 (1/2) (1960) 163.
[16] R. Nitsche, et al. J. Phys. Chem. Solids 21 (3/4) (1961) 199.
[17] A. Castellanos-Gomez, et al. Appl. Phys. Lett. 96 (21.) (2010).
[18] B. Radisavljevic, et al. ACS Nano 5 (2011) 9934.
[19] P. Joensen, et al. Mater. Res. Bull. 21 (4) (1986) 457.
[20] G. Eda, et al. Nano Lett. 11 (12) (2011) 5111.
[21] G. Eda, et al. ACS Nano 6 (8) (2012) 7311.
[22] J.N. Coleman, et al. Science 331 (6017) (2011) 568.
[23] R.J. Smith, et al. Adv. Mater. 23 (34) (2011) 3944.
[24] S. Najmaei, et al. Nat. Mater. 12 (2013) 754.
[25] A.M. van der Zande, et al. Nat. Mater. 12 (6) (2013) 554.
[26] Y. Zhan, et al. Small 8 (7) (2012) 966.
[27] K.-K. Liu, et al. Nano Lett. 12 (3) (2012) 1538.
[28] X. Wang, et al. J. Am. Chem. Soc. 135 (14) (2013) 5304.
[29] Y.-H. Lee, et al. Adv. Mater. 24 (17) (2012) 2320.
[30] A.L. Elías, et al. ACS Nano 7 (2013) 5235.
[31] P. Hohenberg, W. Kohn, Phys. Rev. 136 (3B) (1964) B864.
[32] W. Kohn, L.J. Sham, Phys. Rev. 140 (4A) (1965) A1133.
[33] J.P. Perdew, et al. J. Chem. Theory Comput. 5 (4) (2009) 902.
[34] D.M. Ceperley, B.J. Alder, Phys. Rev. Lett. 45 (7) (1980) 566.
[35] J.P. Perdew, et al. Phys. Rev. Lett. 77 (18) (1996) 3865.
[36] L. Hedin, S. Lundqvist, in: D.T. Frederick Seitz, E. Henry (Eds.), Solid State Physics, vol. 23, Academic Press, New York, 1970, p. 1.
[37] M.S. Hybertsen, S.G. Louie, Phys. Rev. B 34 (8) (1986) 5390.
[38] G. Strinati, Riv. Nuovo Cim. 11 (12) (1988) 1.
[39] M. Rohlfing, S.G. Louie, Phys. Rev. B 62 (8) (2000) 4927.
[40] K.K. Kam, B.A. Parkinson, J. Phys. Chem. 86 (4) (1982) 463.
[41] S.G. Louie, Predicting Materials and Properties: Theory of the Ground and Excited State, Elsevier, Amsterdam, 2006.
[42] T. Li, G. Galli, J. Phys. Chem. C 111 (44) (2007) 16192.
[43] A. Kuc, et al. Phys. Rev. B 83 (24) (2011) 245213.
[44] W. Jin, et al. Phys. Rev. Lett. 111 (10) (2013) 106801.
[45] H.-P. Komsa, A.V. Krasheninnikov, J. Phys. Chem. Lett. 3 (23) (2012) 3652.
[46] Y. Chen, et al. ACS Nano 7 (5) (2013) 4610.
[47] Y. Gong, et al. Nano Lett. 14 (2) (2013) 442.
[48] S.-H. Su, et al. Small 10 (2014) 2589.
[49] S. Bertolazzi, et al. ACS Nano 5 (12) (2011) 9703.
[50] A. Ramasubramaniam, et al. Phys. Rev. B 84 (20) (2011) 205325.
[51] Y. Zhang, et al. Nature 459 (7248) (2009) 820.
[52] J. Feng, et al. Nat. Photon. 6 (12) (2012) 866.
[53] P. Johari, V.B. Shenoy, ACS Nano 6 (2012) 5449.
[54] M. Ghorbani-Asl, et al. Phys. Rev. B 87 (23) (2013) 235434.
[55] W.S. Yun, et al. Phys. Rev. B 85 (3) (2012) 033305.
[56] K. He, et al. Nano Lett. 13 (2013) 2931.
[57] H.J. Conley, et al. Nano Lett. 13 (8) (2013) 3626.
[58] A. Castellanos-Gomez, et al. Nano Lett. 13 (11) (2013) 5361.
[59] Z.Y. Zhu, et al. Phys. Rev. B 84 (15) (2011) 153402.
[60] S.A. Wolf, et al. Science 294 (5546) (2001) 1488.
[61] A. Fert, Rev. Mod. Phys. 80 (4) (2008) 1517.
[62] A. Rycerz, et al. Nat. Phys. 3 (3) (2007) 172.
[63] D. Xiao, et al. Phys. Rev. Lett. 99 (23) (2007) 236809.
[64] D. Xiao, et al. Phys. Rev. Lett. 108 (19) (2012) 196802.
[65] H. Zeng, et al. Nat. Nanotechnol. 7 (2012) 490.
[66] K.F. Mak, et al. Nat. Nanotechnol. 7 (2012) 494.
[67] T. Cao, et al. Nat. Commun. 3 (2012) 887.
[68] K.F. Mak, et al. Science 344 (2014) 1489.
[69] Y. Ding, et al. Physica B 406 (11) (2011) 2254.
[70] A. Ramasubramaniam, Phys. Rev. B 86 (11) (2012) 115409.
[71] Y. Liang, et al. Appl. Phys. Lett. 103 (4) (2013) 042106.
[72] Y. Yoon, et al. Nano Lett. 11 (2011) 3768.
[73] L. Liu, et al. IEEE Trans. Electron Devices 99 (2013) 1.
[74] D. Sarkar, et al. ACS Nano 8 (4) (2014) 3992.
[75] R. Fivaz, E. Mooser, Phys. Rev. 163 (3) (1967) 743.
[76] D. Lembke, A. Kis, ACS Nano 6 (2012) 10070.
[77] S. Kim, et al. Nat. Commun. 3 (2012) 1011.
[78] H. Fang, et al. Nano Lett. 12 (2012) 3788.
[79] W. Liu, et al. Nano Lett. 13 (2013) 1983.
[80] Y. Zhang, et al. Nano Lett. 12 (3) (2012) 1136.
[81] S. Jo, et al. Nano Lett. 14 (2014) 2019.
[82] D. Braga, et al. Nano Lett. 12 (10) (2012) 5218.
[83] J.T. Ye, et al. Science 338 (6111) (2012) 1193.
[84] B. Radisavljevic, A. Kis, Nat. Mater. 12 (2013) 815.
[85] B. Baugher, et al. Nano Lett. 13 (9) (2013) 4212.
[86] V.K. Sangwan, et al. Nano Lett. 13 (9) (2013) 4351.
[87] X. Xie, et al. ACS Nano 13 (2014) 5633.
[88] F. Schwierz, Nat. Nanotechnol. 6 (3) (2011) 135.
[89] K. Kaasbjerg, et al. Phys. Rev. B 85 (11) (2012) 115317.
[90] K. Kaasbjerg, et al. Phys. Rev. B 87 (23) (2013) 235312.
[91] X. Li, et al. Phys. Rev. B 87 (11) (2013) 115418.
[92] Z.-Y. Ong, M.V. Fischetti, Phys. Rev. B 88 (16) (2013) 165316.
[93] N. Ma, D. Jena, Phys. Rev. X 4 (1) (2014) 011043.
[94] W. Zhu, et al. Nat. Commun. 5 (2014).
[95] J. Brivio, et al. Nano Lett. 11 (2011) 5148.
[96] P. Miró, et al. Adv. Mater. 25 (38) (2013) 5473.
[97] H. Liu, et al. ACS Nano 6 (10) (2012) 8563.
[98] S. Das, et al. Nano Lett. 13 (1) (2012) 100.
[99] B. Radisavljevic, et al. Appl. Phys. Lett. 101 (2012) 043103.
[100] H. Wang, et al. Nano Lett. 12 (9) (2012) 4674.
[101] S. Bertolazzi, et al. ACS Nano 7 (2013) 3246.
[102] Z. Yin, et al. ACS Nano 6 (1) (2012) 74.
[103] H.S. Lee, et al. Nano Lett. 12 (2012) 3695.
[104] O. Lopez-Sanchez, et al. Nat. Nanotechnol. 8 (7) (2013) 497.
[105] M.A. Krainak, et al. SPIE Proc. (2010) 76810Y.
[106] M. Buscema, et al. Nano Lett. 13 (2013) 358.
[107] R.S. Sundaram, et al. Nano Lett. 13 (4) (2013) 1416.
[108] A. Pospischil, et al. Nat. Nanotechnol. 9 (4) (2014) 257.
[109] B.W.H. Baugher, et al. Nat. Nanotechnol. 9 (4) (2014) 262.
[110] J.S. Ross, et al. Nat. Nano 9 (4) (2014) 268.

Please cite this article in press as: O.V. Yazyev, A. Kis, Mater. Today (2014), http://dx.doi.org/10.1016/j.mattod.2014.07.005

[111] Y.J. Zhang, et al. Science 344 (2014) 725.
[112] A. Kormányos, et al. Phys. Rev. B 88 (4) (2013) 045416.
[113] H. Rostami, et al. Phys. Rev. B 88 (8) (2013) 085440.
[114] L. Britnell, et al. Science 335 (6071) (2012) 947.
[115] T. Georgiou, et al. Nat. Nanotechnol. 8 (2012) 100.
[116] L. Britnell, et al. Science 340 (2013) 1311.
[117] M. Bernardi, et al. Nano Lett. 13 (8) (2013) 3664.
[118] J. Li, et al. J. Phys. Chem. C 117 (30) (2013) 15842.
[119] H.-Y. Chang, et al. ACS Nano 7 (2013) 5446.
[120] G.A. Salvatore, et al. ACS Nano 7 (10) (2013) 8809.
[121] G.-H. Lee, et al. ACS Nano 7 (9) (2013) 7931.
[122] J. Pu, et al. Nano Lett. 12 (8) (2012) 4013.
[123] A. Castellanos-Gomez, et al. Adv. Mater. 25 (46) (2013) 6719.
[124] A.K. Geim, I.V. Grigorieva, Nature 499 (7459) (2013) 419.

Please cite this article in press as: O.V. Yazyev, A. Kis, Mater. Today (2014), http://dx.doi.org/10.1016/j.mattod.2014.07.005